Frontiers of Environmental Science & Engineering
2025, 19(4): 51 https://doi.org/10.1007/s11783-025-1971-1

RESEARCH ARTICLE

Highly recyclable EDTA-crosslinked chitosan-gelatin biopolymer adsorbent for separation and recovery of rare earth elements from aqueous solution

Monu Verma[1], Deepa Sachan[1], Vinod Kumar[2,5], Waseem Ahmad[4], Nishesh Sharma[3], Hyunook Kim ✉ [1]

1. Water-Energy Nexus Laboratory, Department of Environmental Engineering, University of Seoul, Seoul 02504, Republic of Korea
2. Department of Food Science & Technology, Graphic Era (Deemed to Be University), Dehradun Uttarakhand 248002, India
3. Department of Chemistry, Uttaranchal University, Dehradun Uttarakhand 248007, India
4. Department of Chemistry, Graphic Era (Deemed to Be University), Dehradun, Uttarakhand 248002, India
5. Peoples' Friendship University of Russia (RUDN University), Moscow 117198, Russian Federation

HIGHLIGHTS

- Chitosan gelatin crosslinked biopolymer was used for REEs separation and recovery.
- Rate constant (k_2) was obtained as (9.60–10.30) × 10^{-4} g/(mg·min) for used REEs.
- Monolayer adsorption capacities were 76.70–86.20 mg/g for used REEs.
- β for Eu(III) separation was 1.383 and 1.322 for Eu/Sc and Eu/Yb.
- Adsorption and separation were due to electrostatics and complexation with REEs.

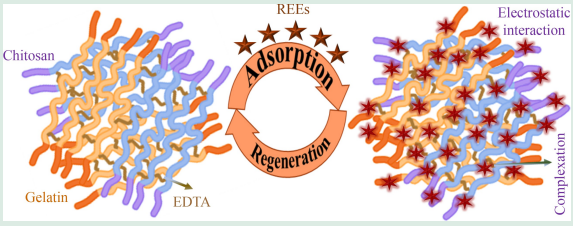

ABSTRACT: A biopolymer adsorbent was prepared by crosslinking chitosan (CS) and gelatin (GL) with ethylenediaminetetraacetic acid (EDTA) for the separation and recovery of three famous rare earth elements (REEs), i.e., lanthanum (La(III)), cerium (Ce(III)), and europium (Eu(III)), from water. In this adsorbent, the EDTA moiety acts as a crosslinking agent, in addition to aiding in REE adsorption via coordination sites. Various parameters, including contact time, pH, initial REE concentration, reusability, and selectivity, were investigated during the REE recovery from water. The kinetic results fit better with the pseudo-second-order (PSO) kinetics model, confirming the involvement of chemisorption and external film diffusion in the rate-determining step. The isotherm data fit the Langmuir model, indicating a homogeneous surface for REE adsorption. The rate constant (k_2) values for PSO kinetics were (9.60 ± 0.05) × 10^{-4}, (8.67 ± 0.04) × 10^{-4}, and (10.30 ± 0.04) × 10^{-4} g/(mg·min), while the maximum adsorption capacities were 76.70 ± 5.70, 79.10 ± 6.80, and 86.20 ± 5.10 mg/g for La(III), Ce(III), and Eu(III), respectively. The CS-EDTA-GL adsorbent provided a good separation factor (β) in 16 REE

✉ Corresponding author. E-mail: h_kim@uos.ac.kr
Article history: Received 22 August 2024, Revised 16 January 2025, Accepted 17 January 2025, Available online 28 February 2025

mixtures; among them, an optimal β was observed for Eu(III) with values of 1.3838, 1.322, 1.284, 1.351, 1.4896, and 1.2792 for Eu/Sc, Eu/Yb, Eu/Tm, Eu/Y, Eu/La, and Eu/Er, respectively. Adsorption mechanism confirms the electrostatic interactions and coordination complexation role in the REE adsorption. Finally, the adsorbent was used in pure water, tap water, and two industrial wastewater samples collected at real environmental concentrations to determine its suitability for practical applications.

KEYWORDS: Adsorption recovery, Rare earth elements, Separation factor, Industrial wastewater, Recovery mechanism

1 Introduction

Rare earth elements (REEs), also known as rare earth metals (REMs), are crucial in modern science and technology. They are widely used in various applications, including batteries, communication devices, electric car engines, wind turbines, and optical devices, and their global industrial demand is increasing rapidly (Unsworth et al., 2020). However, the global supply of REEs is uncertain and poses significant risk, as 95% of the supply is controlled by China, despite sufficient reserves being available worldwide. This position of dominance is due to China's advanced REE processing technologies and production facilities (Brewer et al., 2019; Kegl et al., 2020). Therefore, high demand and limited supply have motivated the research community to focus on separating and recovering REEs from industrial and municipal waste streams.

Various technologies, including solvent extraction, ion exchange, membrane separation, chemical precipitation, and adsorption, have been used for the separation and recovery of REEs from aqueous media (Rahman et al., 2011; Li et al., 2018; Maes et al., 2017). However, these technologies are generally expensive, environmentally harmful, involve high chemical and energy consumption, and are inefficient at handling low concentrations of REEs (Jun et al., 2023; Pathapati et al., 2023). Adsorption is considered an alternative green method for REE separation and recycling owing to its low cost, simplicity, high efficiency, and zero waste by-product production (Xie et al., 2022; Yan et al., 2023). Currently, a range of adsorbents are used to remove REEs from aqueous solutions, including porous carbon (Brown and Balkus, 2021; Gismondi et al., 2022), metal oxides (Dupont et al., 2014), biopolymer composites (Wu et al., 2022), and zeolites (Ji and Zhang, 2022). Recently, honeycomb-shaped covalent organic frameworks, synthesized using eutectic solvents (DES), were reported for the selective adsorption of REEs from aqueous solutions (Xiao et al., 2022). Additionally, Yan et al. (2023) developed bio-nanoparticles (BC@FeNPs-EPS) by incorporating Fe nanoparticles into extracellular polymeric substances produced by *Bacillus cereus* to demonstrate the efficient removal of Eu(III) from mine wastewater. As previously mentioned, research continues to focus on the development of organic and inorganic polymeric adsorption materials. Nonetheless, the challenges in achieving selectivity, high removal efficiency, and recovery of REEs at environmentally relevant concentrations remain critical and must be addressed urgently.

Chitosan (CS) and gelatin (GL) are natural, environment-friendly, and biodegradable polymers that have attracted significant attention owing to their $-NH_2$, $-COOH$, and $-OH$ functional groups, which provide outstanding adsorption capacities for metal ions via electrostatic attraction or chemical chelation (Lone et al., 2019). However, these polymers are limited to wastewater treatment owing to their solubility in acidic environments, poor chemical resistance, swelling in aqueous solutions, and difficulties in separation using conventional methods, such as filtration and centrifugation (Roosen and Binnemans, 2014; Lone et al., 2019). To address these issues, functionalization and crosslinking have been explored using various reagents, such as glutaraldehyde (Hamza et al., 2022; Verma et al., 2023), N-isopropylacrylamide (Ren et al., 2023), 1-ethyl-3-(3-dimethylaminopropyl)-carbodiimide hydrochloride (EDC) (Aoki et al., 2003), and epichlorohydrin (EPI) (Li et al., 2016). Particularly, diethylenetriaminepentaacetic acid (DTPA) or ethylenediaminetetraacetic acid (EDTA) groups have been reported as good crosslinking agents that improve the REE adsorption efficiency of CS and prevent its dissolution in acidic media (Roosen and Binnemans, 2014). Furthermore, EDTA has garnered significant interest because it acts not only as a crosslinking agent but also as a binding site for metal ions. Additionally, EDTA is a more affordable and less harmful alternative to traditional crosslinkers, such as EPI and EDC,

making it a promising choice for REE recovery applications. Roosen and Binnemans (2014) reported the functionalization of CS with EDTA to yield less soluble properties and provide efficient coordinated binding sites for the adaptive removal of REEs from water. They employed a medium-pressure liquid chromatographic column to separate REEs (Pr^{3+}/Nd^{3+}, Nd^{3+}/Ho^{3+}, and Pr^{3+}/Nd^{3+}/Ho^{3+}) with a stationary phase composed of EDTA-CS/silica and a mobile phase of dilute nitric acid. Similarly, Zhao et al. (2016) reported a cross-linked biopolymer, β-cyclodextrin with EDTA, and employed it for the adsorption of lanthanum (La(III)), cerium (Ce(III)), and europium (Eu(III)) from water; they found that the synthesized adsorbent had homogenous surface and adsorption capacities of 0.34, 0.35, and 0.36 mmol/g, respectively. Feng et al. (2021) further advanced this approach by modifying CS with EDTA and a zeolite imidazole framework (ZIF) to recover La(III), Eu(III), and Yb(III) from aqueous solution.

This study aimed to develop a cross-linked CS-GL adsorbent using EDTA as the crosslinker (CS-EDTA-GL) for the efficient separation and recovery of three trivalent REEs, La(III), Ce(III), and Eu(III), from water. Various parameters, including the contact time, pH, initial REE concentrations, reusability, and selectivity, were systematically investigated to optimize the recovery of REEs. Subsequently, adsorption isotherm and kinetic models were formulated and applied to the experimental data to investigate the REE adsorption mechanism of the synthesized material. To support the proposed mechanism, elemental mapping, distribution, FT-IR, and XPS were employed. Finally, the REE-recovery performance of the prepared adsorbent was investigated in pure water, tap water, and two industrial wastewater at various environmental concentrations to assess its feasibility for practical applications.

2 Materials and methods

2.1 Chemicals and reagents

All chemicals and reagents used in the experiments are described in the Supplementary Material (Text SI−1).

2.2 Synthesis of CS-EDTA-GL polymer

The biopolymeric adsorbent CS-EDTA-GL was prepared by modifying a previously reported method (Verma et al., 2022a). To optimize the synthesis conditions, three different ratios of CS to GL (1:1, 2:1, and 1:2) were crosslinked with 25 g EDTA dianhydride (Fig. S1, Supplementary Material). This synthetic process has been reported to provide the best yield. In brief, 2.5 g of CS was dissolved in 50 mL of a 10% acetic acid solution at 50 °C, which was vigorously mixed for an hour with another solution prepared by dissolving 5.0 g of GL in 25 mL of deionized (DI) water at 40 °C. The resulting mixture was diluted 6-fold with methanol at room temperature and stirred continuously for 3 h. Subsequently, 25 g EDTA dianhydride, prepared according to the previously reported method (Tülü and Geckeler, 1999), was dispersed in 50 mL methanol and gradually added to the CS-GL solution with vigorous stirring for 24 h at 25 °C. The resulting precipitate was filtered and vigorously stirred in ethanol for 16 h. After another filtration, the product was washed sequentially with NaOH solution (pH ~11.0), followed by four washes with DI water, 0.1 mol/L HCl, DI water, and finally with ethanol. The produced biopolymer was freeze-dried (−75 °C) in ilShinBiobase (TFD8503 model, Seoul, Republic of Korea) under high-vacuum conditions for 72 h and stored in a desiccator until use. The overall synthesis of the CS-EDTA-GL adsorbent is shown in Scheme 1.

2.3 Adsorbent characterization

The detailed characterizations of the adsorbent are provided in Text SI−2.

2.4 Batch adsorption experiments

The details of all batch adsorption experiments, including adsorption in multi-component REE systems, reusability tests, selectivity tests, and the performance of CS-EDTA-GL in recovering target REEs from DI water, tap water, and industrial wastewater at an environmentally relevant concentration, are discussed in Text SI−3.

3 Results and discussion

3.1 Characterization

Various characterization techniques were used to investigate the different properties of the synthesized CS-EDTA-GL adsorbents. The FESEM morphology is shown in Fig. 1(a), revealing rough surfaces with irregular small sheets and crack-like structures, along with high porosity, which would be beneficial for REE adsorption. The FT-IR spectra of the raw materials with

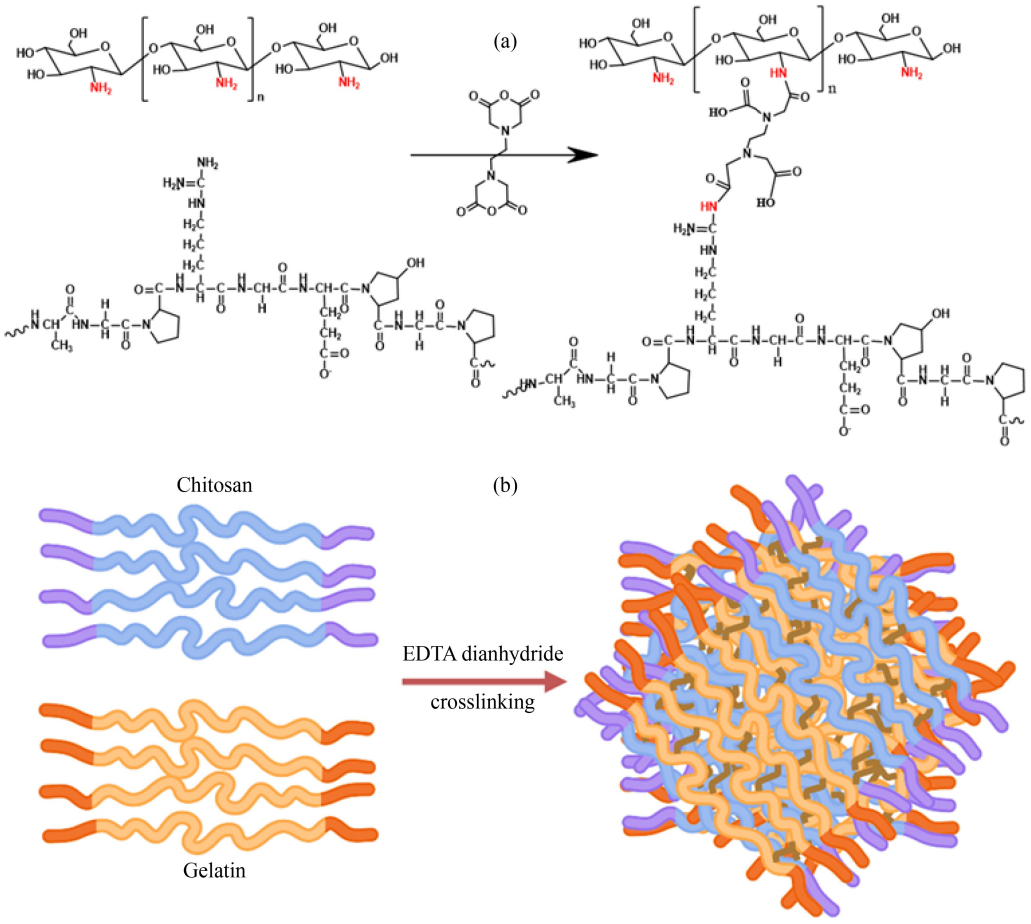

Scheme 1 Synthesis procedure of CS-EDTA-GL adsorbent via EDTA crosslinking (a), and schematic presentation of the CS-EDTA-GL formation (b).

the cross-linked CS-EDTA-GL adsorbent are presented in Fig. 1(b), displaying the characteristic peaks associated with CS, GL, and EDTA, as reported previously (Perumal et al., 2019; Verma et al., 2022a). Additionally, the prepared CS-EDTA-GL exhibited important characteristic peaks situated at 1643 cm^{-1} (C=O stretching vibrations in the −CONH− amide bond), 1523 cm^{-1} (−NH− deformation of the amide group), and 1737 cm^{-1} (C=O of the new carboxyl group insertion) (Repo et al., 2010; Zhao et al., 2017; Chen et al., 2019). These peaks confirm that CS and GL were successfully crosslinked with EDTA. To check the crystalline nature, XRD data of the raw materials and crosslinked adsorbent were collected and are presented in Fig. 1(c). As shown in the figure, CS exhibits two distinct peaks at 9.57° and 19.85°, indicating a partially crystalline nature. In contrast, GL exhibited only a broad hump-type peak between 10° and 24°, signifying its primarily amorphous character. As previously reported by our research group (Verma et al., 2022a), the IR spectrum of EDTA consists of several sharp peaks, confirming its highly crystalline structure. However, the CS-EDTA-GL adsorbent displayed a single broad hump-type peak between 10° and 35°, with a higher intensity than the CS and GL raw materials and the disappearance of individual peaks of the raw materials, confirming the insertion of EDTA into the polymeric structure through the crosslinking reaction. The N_2 adsorption–desorption isotherm for the CS-EDTA-GL adsorbent is shown in Fig. 1(d), exhibiting a type IV isotherm with an H3 hysteresis loop, possibly due to the mesoporous materials with capillary condensation properties. The BET surface area, average pore diameter, and total pore volume were 17.051 m^2/g, 19.594 nm, and 0.0835 cm^3/g, respectively. The Barrett–Joyner–Halenda (BJH) pore size distribution, corresponding to the N_2 adsorption–desorption isotherm, is displayed in the inset of Fig. 1(d), clearly showing a wide pore size distribution. The thermal stability of the CS-EDTA-GL adsorbent was investigated by TGA (Fig. S2). The figure clearly shows the decomposition of the adsorbent in three

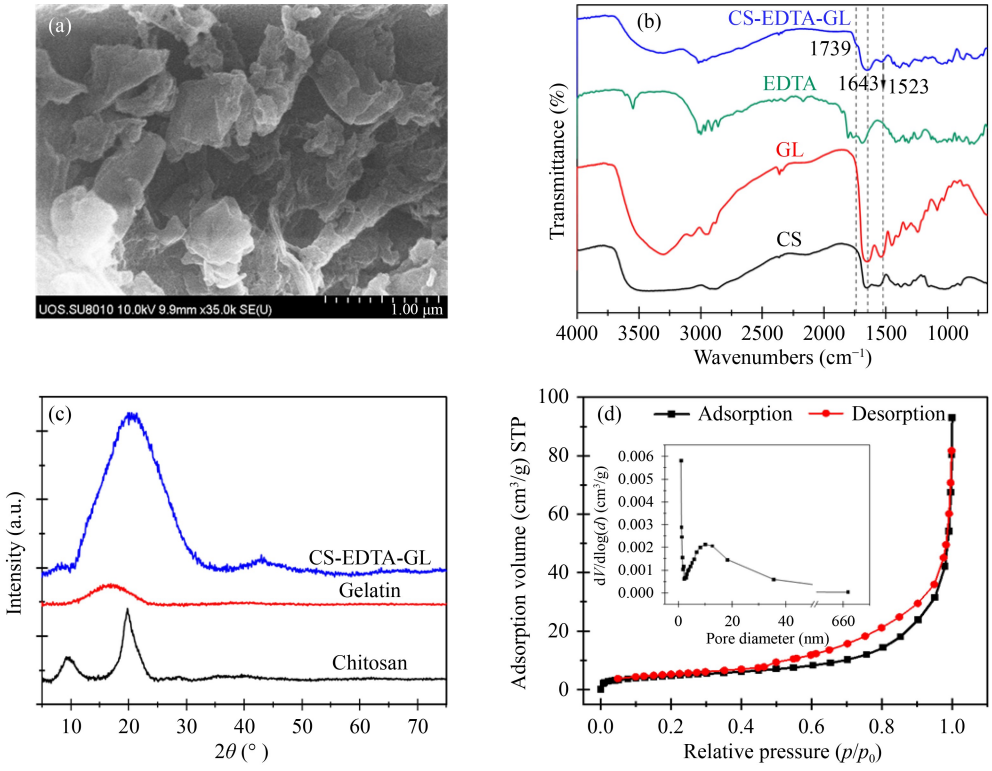

Fig. 1 FESEM image (a), FT-IR spectra (b), XRD patterns (c), and N_2 adsorption-desorption isotherm and pore size distribution (inset) (d) of the CS-EDTA-GL adsorbent.

steps. The first step weight loss between 25 and 110 °C was due to moisture removal. The second step weight loss between 220 and 370 °C was due to the decomposition of EDTA. The final stage of weight loss up to 800 °C was due to the decomposition of existing polysaccharides and proteins (CS and GL). Additionally, the DTG curve clearly shows three pyrolysis steps, which were confirmed by the peaks situated at 53.40, 279.90, and 392.65 °C.

3.2 Effect of pH

The pH is a critical factor in obtaining the maximum REE recovery through the adsorption process. The pH dependency of REE adsorption onto the CS-EDTA-GL adsorbent is shown in Fig. 2(a), which reveals a clear increasing trend in REE recovery with increasing pH. This behavior is consistent with previously reported studies on the recovery of various REEs using different adsorbents, such as EDTA- and DTPA-functionalized CS (Roosen and Binnemans, 2014), TpPa COFs (Xiao et al., 2022), and DNA-functionalized mesoporous carbon (Xiao et al., 2022). The data also indicate that REE adsorption onto the CS-EDTA-GL adsorbent at a pH of 1 was relatively low; however, as the pH increased from 2 to 5, the adsorption capacity of CS-EDTA-GL increased rapidly and reached equilibrium at a pH of 6. This behavior was strongly supported by the isoelectric point of CS-EDTA-GL (pH_{PZC} = 3.6), as shown in Fig. S3. The pH_{PZC} of the CS-EDTA-GL was determined using the pH drift method and was found to be significantly lower than those of CS (pH_{PZC} = 9.0) and GL (pH_{PZC} = 4.6) (Johlin, 1930; Sirviö et al., 2021). This reduction in the pH_{PZC} can be attributed to the presence of carboxylic groups introduced by EDTA during the crosslinking process. At low pH values, particularly below the isoelectric point, the adsorbent surface is positively charged, leading to electrostatic repulsion with the positively charged REEs, resulting in a low adsorption capacity. As the pH increases, the adsorbent surface becomes neutral, decreasing the electrostatic repulsion barrier and increasing the adsorption capacity. When the pH increases beyond the isoelectric point of the adsorbent, its surface becomes negatively charged, and electrostatic interactions with positively charged REEs increase, resulting in a high adsorption capacity, as illustrated in Fig. 2(a). This observation clearly indicates that high adsorption capacities can be achieved at high solution pH values, leading to the selection of a pH of 6.0 for further experiments. Here, we note that at a pH of 5.0, all EDTA groups are not fully deprotonated for REE

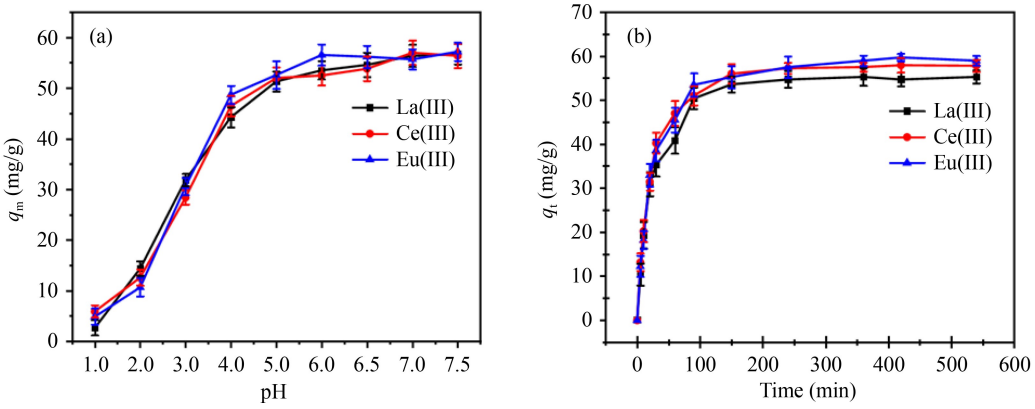

Fig. 2 Effects of pH (a) and contact time (b) on the adsorption of REEs onto CS-EDTA-GL.

adsorption owing to the pKa_5 value of 6.1 for EDTA. However, adsorption reached near equilibrium at a pH of 5.0, possibly owing to the combined adsorption effects of CS and GL, in addition to the ion exchange process (Roosen and Binnemans, 2014).

3.3 Kinetics analysis

The adsorption capacity of the synthesized CS-EDTA-GL for REE recovery was evaluated as a function of time to determine the equilibrium time and adsorption kinetics, as illustrated in Fig. 2(b). The results clearly show a rapid increase in adsorption capacity within the first 20–30 min and reached up to 30–34 mg/g. After the initial phase, the adsorption rate decreased and reached equilibrium within 90 min. This rapid adsorption in the initial stage may be due to the significant availability of adsorption sites on the CS-EDTA-GL surface, which facilitated efficient REE recovery. Similar types of adsorption trends have been previously observed in studies on EDTA-functionalized *β*-cyclodextrin and CS (EDTA-β-CD & EDTA-CS) for REE recovery (Roosen and Binnemans, 2014; Zhao et al., 2016). Based on the kinetic data, a contact time of 300 min was selected for further experiments to ensure complete adsorption.

To further understand the rate-determining step and adsorption mechanism, three well-known kinetic models–the pseudo-first-order (PFO), pseudo-second-order (PSO), and Webber–Morris intraparticle diffusion models–were applied to the data obtained from the adsorption of REEs by CS-EDTA-GL. A detailed discussion of these models is provided in Text SI–4.1. Figure 3 displays the nonlinear kinetic fitting of the experimental data, and the relevant fitting parameter values are summarized in Table 1. The results clearly indicate that the PSO kinetic model fitted better than the PFO, as higher correlation coefficients (R^2) of 0.992, 0.997, and 0.995 for La(III), Ce(III), and Eu(III) were obtained compared to those of PFO, i.e., 0.983, 0.984, and 0.982, respectively. Moreover, the calculated equilibrium adsorption capacities ($q_{e,cal}$) of the synthesized adsorbent from the PSO models (i.e., 57.80 ± 0.90, 61.0 ± 0.60, and 62.40 ± 0.80 mg/g for La(III), Ce(III) and Eu(III), respectively) were significantly closer to the experimental values ($q_{e,exp}$) (55.70 ± 1.50,

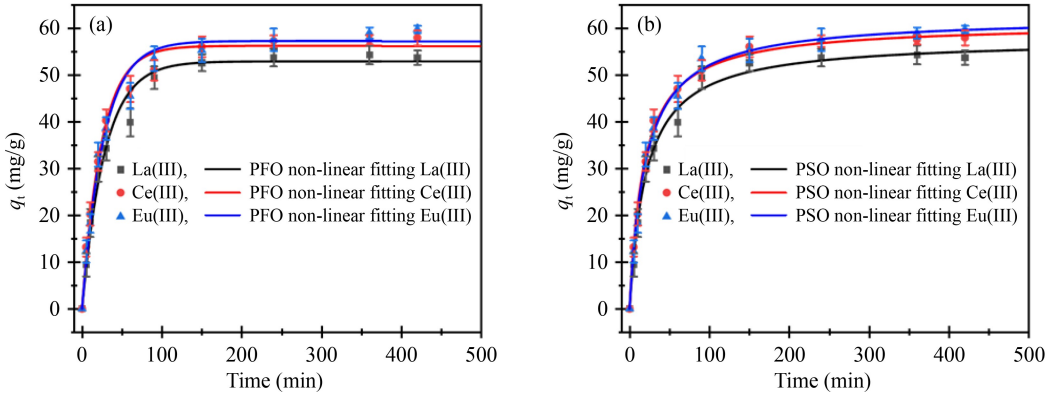

Fig. 3 Nonlinear fitting for PFO (a) and PSO (b) in the REE adsorption onto CS-EDTA-GL.

Table 1 Kinetics modeling parameters for REE adsorption onto CS-EDTA-GL adsorbent

Models	Parameters	REEs		
		La(III)	Ce(III)	Eu(III)
PFO	$q_{e,exp}$ (mg/g)	55.70 ± 1.50	57.90 ± 1.60	59.70 ± 1.10
	$q_{e,cal}$ (mg/g)	52.90 ± 1.10	53.20 ± 0.90	52.20 ± 1.10
	k_1 (min^{-1})	0.0351 ± 0.0031	0.0405 ± 0.0029	0.0371 ± 0.0029
	R^2	0.983	0.984	0.982
PSO	$q_{e,cal}$ (mg/g)	57.80 ± 0.90	61.0 ± 0.60	62.40 ± 0.80
	k_2 (g/(mg·min))	(9.60 ± 0.76) × 10^{-4}	(8.67 ± 0.50) × 10^{-4}	(10.30 ± 0.56) × 10^{-4}
	R^2	0.992	0.997	0.995
Intra-particle diffusion	$k_{i,1}$ (mg/(g·$min^{0.5}$))	6.80 ± 0.60	7.40 ± 0.40	7.30 ± 0.70
	C	–1.66 ± 2.07	–1.60 ± 1.73	–2.0 ± 2.30
	R^2	0.978	0.990	0.977
	$k_{i,2}$ (mg/(g·$min^{0.5}$))	2.85 ± 0.54	2.31 ± 0.20	3.68 ± 0.43
	C	20.10 ± 4.70	28.36 ± 1.88	17.92 ± 3.35
	R^2	0.932	0.984	0.986
	$k_{i,3}$ (mg/(g·$min^{0.5}$))	0.13 ± 0.05	0.16 ± 0.04	0.44 ± 0.079
	C	52.30 ± 0.90	54.40 ± 0.80	49.91 ± 1.40
	R^2	0.707	0.824	0.887

57.90 ± 1.60, and 59.70 ± 1.10 mg/g for La(III), Ce(III), and Eu(III), respectively). These results confirm that REE recovery using CS-EDTA-GL is governed by chemisorption, which is the rate-determining step (Park et al., 2020). Moreover, higher rate constant (k_2) values for Eu(III) indicate a faster adsorption rate than those of La(III) and CE(III), which is likely owing to the smaller radius of Eu(III) (Zhao et al., 2016).

To better understand the diffusion mechanism between REEs and the synthesized CS-EDTA-GL adsorbent, the Weber–Morris intraparticle diffusion model was applied to the kinetic data. The results are presented in Fig. S4 and Table 1, illustrating three distinct linear stages of adsorption: 1) external or boundary diffusion, during which REEs were rapidly adsorbed onto the active sites of the adsorbent surface; 2) intraparticle diffusion, during which REEs gradually diffused into the pores of the adsorbent's interior structure from the nearly saturated adsorbent's exterior surface; and 3) equilibrium, during which no further adsorption or diffusion of REEs was observed. The results show that the order of the intraparticle diffusion rate constants (k_i) was $k_{i,1} > k_{i,2} > k_{i,3}$, and the $k_{i,1}$ values were significantly higher than the $k_{i,2}$ and $k_{i,3}$ values, clearly confirming that intraparticle diffusion was not the rate-controlling stage and that the surface diffusion step may be the rate-determining step (Zhang et al., 2022).

3.4 Adsorption isotherm

To investigate the adsorption behavior and maximum adsorption capacity (q_m) of the CS-EDTA-GL adsorbent for REE recovery, the Langmuir and Freundlich isotherm models were applied to the adsorption equilibrium data. Text SI−4.2 describes the details of these models.

Figure 4 and Table 2 present the nonlinear fitting results and parameter values, respectively. The Langmuir model showed higher R^2 values of 0.991, 0.984, and 0.994 than the Freundlich fit, with R^2 values of 0.939, 0.906, and 0.946 for La(III), Ce(III), and

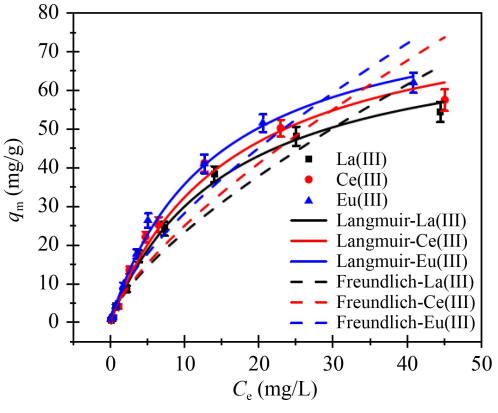

Fig. 4 Nonlinear Langmuir and Freundlich isotherm fitting plots in the REE adsorption onto the CS-EDTA-GL adsorbent.

Eu(III), respectively. Additionally, the Langmuir model provided a better curve fitting to the experimental data and produced calculated maximum adsorption capacities ($q_{m,cal}$) closer to the experimental $q_{m,exp}$ values (Table 2) than those from the Freundlich model. Therefore, the Langmuir model accurately fits the REE adsorption data for the CS-EDTA-GL adsorbent. This indicates that the synthesized adsorbent possesses a homogeneous adsorption surface with identical sites in the form of EDTA, −OH, and $-NH_2$ groups, which have the same adsorption affinity for REEs. As the adsorption affinity was the same in this model, the adsorbed REEs did not compete or react with each other, resulting in monolayer adsorption. The adsorption capacities calculated from the Langmuir model were 76.70 ± 5.70, 79.10 ± 6.80, and 86.20 ± 5.10 mg/g for La(III), Ce(III), and Eu(III), respectively. The higher adsorption capacity for Eu(III) in comparison to La(III) and (Ce(III) might be due to EDTA having a higher stability constant with Eu(III) (17.3) than with La(III) (15.5) and Ce(III) (15.9). This stability constant was also supported by the Langmuir constant results (Table 2). From the Freundlich model, the relative strength, "n" was greater than 1, confirming the favorable adsorption process. Moreover, the adsorption capacities for heavy metals were greater than those of REEs with EDTA-containing adsorbents, as previously reported (Verma et al., 2022b; 2022d), and this might be due to higher stability constants (log K) for heavy metal(II)-EDTA complexes than for lanthanide(III)-EDTA complexes (Roosen and Binnemans, 2014; Zhang et al., 2022).

3.5 Adsorption in ternary-component system

Generally, REEs or metals rarely exist in single-component systems (Vijayaraghavan et al., 2011). Therefore, it is interesting to explore the performance of the CS-EDTA-GL adsorbent under competitive conditions for multi-component REE adsorption. Details of the experiment are provided in Text SI−3.2. In multi-component systems, three scenarios are possible: if $q_{mix}/q_{single} > 1$, adsorption is promoted by the presence of competing REEs; if $q_{mix}/q_{single} < 1$, adsorption is suppressed by the presence of competing REEs; and if $q_{mix}/q_{single} = 1$, adsorption is unaffected by the presence of competing REEs.

Figure S5 shows the effects of other competing ions on REE adsorption, clearly showing a q_{mix}/q_{single} value of less than 1, which confirms the suppression of REE adsorption in the presence of competing lanthanides. The Langmuir-calculated q_{mix} values for La(III), Ce(III), and Eu(III) were 12.10 ± 2.40, 16.30 ± 3.40, and 34.30 ± 4.70 mg/g, respectively, indicating more adsorption inhibition of La(III) and Ce(III) adsorption compared to Eu(III) in the ternary mixture. This adsorption inhibition effect can be explained using Pearson's hard-soft acid-base (HSAB) theory, which posits that hard acids bind more strongly to hard bases, and soft acids bind more strongly to soft bases (Pearson, 1963). In comparison to the single-component system, isotherm parameter values, such as q_m, K_L, and n, were also affected in the multi-component system due to a reduction in the adsorption capacity.

In the single-component system, the adsorption recovery order of REEs by CS-EDTA-GL was La(III) < Ce(III) < Eu(III), which was due to the varying stability constants of the different lanthanides. However, the differences in the adsorption capacities for the three lanthanides were not significant. In contrast, in the ternary-component system, the difference in the adsorption capacity was significantly higher, and Eu(III) was adsorbed more rapidly than La(III) and Ce(III), as listed in Table 3. This can be explained using water structure constants, which are based on the electron affinity sequence in a multi-component system (Vijayaraghavan et al., 2011). The water structure

Table 2 Parameters for isotherms of REE adsorption onto CS-EDTA-GL in a single-component system

Models	Parameters	REEs		
		La(III)	Ce(III)	Eu(III)
Langmuir isotherm	$q_{m,exp}$ (mg/g)	54.50 ± 3.0	57.80 ± 2.90	62.0 ± 2.80
	$q_{m,cal}$ (mg/g)	76.70 ± 5.70	79.10 ± 6.80	86.20 ± 5.10
	K_L (L/mg)	0.0637 ± 0.0085	0.0622 ± 0.0122	0.0718 ± 0.0077
	R^2	0.991	0.984	0.994
Freundlich isotherm	K_F (mg/g) (L/mg)$^{1/n}$	4.6237 ± 0.8348	4.7433 ± 1.0113	5.9101 ± 1.005
	n	1.42 ± 0.12	1.38 ± 0.14	1.47 ± 0.12
	R^2	0.939	0.906	0.946

Table 3 Parameters for the isotherms of REE adsorption onto CS-EDTA-GL in the ternary component system

Models	Parameters	REEs		
		La(III)	Ce(III)	Eu(III)
Langmuir isotherm	$q_{m,exp}$ (mg/g)	10.80 ± 1.80	16.10 ± 2.0	31.20 ± 2.40
	$q_{m,cal}$ (mg/g)	12.10 ±2.40	16.30 ± 3.40	34.30 ± 4.70
	K_L (L/mg)	0.2752 ± 0.1347	0.1346 ± 0.0630	0.0723 ± 0.0221
	R^2	0.955	0.966	0.968
Freundlich isotherm	K_F (mg/g) (L/mg)$^{1/n}$	2.6197 ± 0.9017	2.9045 ± 0.8485	2.7686 ± 0.9892
	n	2.61 ± 0.75	2.26 ± 0.45	1.65 ± 0.27
	R^2	0.788	0.881	0.874

constants for Eu(III), Ce(III), and La(III) were in the range of 0.75 to 0.78; higher values indicate lower affinity. As a result, the combination of higher stability constant and lower water structure constant creates a better affinity gap for Eu(III) than for Ce(III) and La(III). A similar trend for Yb(III) < La(III) < Ce(III) < Eu(III) was reported for a four-component system with brown marine algae (Vijayaraghavan et al., 2011).

3.6 Adsorption separation of REEs

To evaluate the effectiveness of CS-EDTA-GL for REE separation, an adsorption experiment was conducted using a mixture of 16 REEs with equal concentrations of each ion to determine the separation factor and selectivity. Details of the experiment are provided in Text SI−3.3.

Figure 5 illustrates the β values of CS-EDTA-GL for the adsorption of REEs, highlighting its enhanced selectivity for Eu(III), followed by Ce(III). The β values for the Eu(III) pairs were 1.383, 1.322, 1.284, 1.351, 1.489, and 1.279 for Eu/Sc, Eu/Yb, Eu/Tm, Eu/Y, Eu/La and Eu/Er, respectively. Similarly, the β values for Ce(III) pairs were 1.339, 1.107, 1.112, 1.301, and 1.401 for Ce/Yb, Ce/La, Ce/Dy, Ce/Tm, and Ce/Sc, respectively. These values are sufficient to suggest the feasibility of industrial applications for REE separation, indicating that CS-EDTA-GL exhibits good separation efficiency and selectivity for the different existing REEs. However, β values are < 1 for certain pairs, indicating that the separation conditions would not be significantly sufficient for REEs of equal concentrations. Nevertheless, CS-EDTA-GL demonstrates significant potential for the separation of

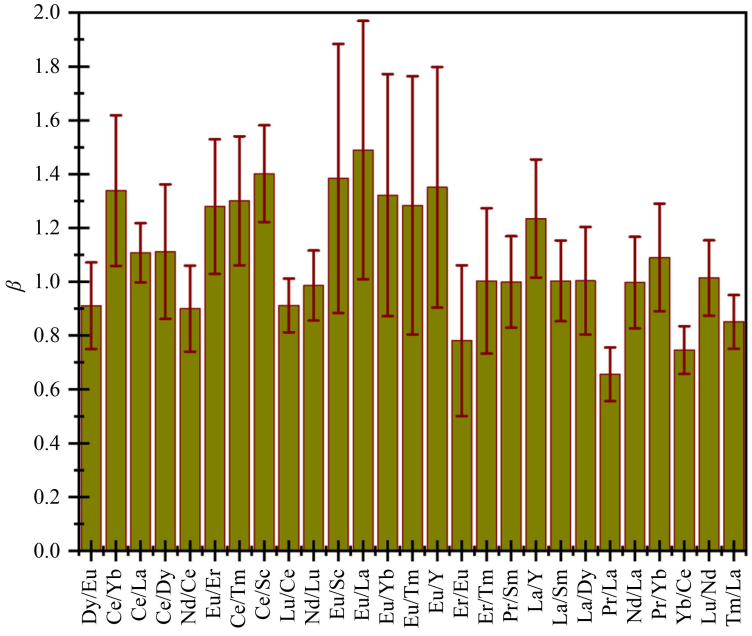

Fig. 5 Separation factor between some REEs onto the CS-EDTA-GL adsorbent.

Eu(III) and Ce(III). Furthermore, we investigated the regeneration and stability of the CS-EDTA-GL adsorbent for practical applications.

3.7 Regeneration and stability analysis

In addition to regeneration, reusability is a crucial parameter for evaluating the stability and long-term performance of adsorbents. Therefore, CS-EDTA-GL was regenerated using 1.0 mol/L HNO_3 for five continuous adsorption–desorption cycles, and the results are presented in Fig. 6(a). The results indicated an approximately 99% regeneration efficiency in the first cycle for La(III), Ce(III), and Eu(III), suggesting that HNO_3 is an effective solvent for regenerating adsorbents and recovering REEs from water. Even after five consecutive adsorption–desorption cycles, the regeneration efficiencies remained at 89.20%, 87.90%, and 90.80% for La(III), Ce(III), and Eu(III), respectively, confirming the optimal stability of the CS-EDTA-GL adsorbent in an HNO_3 solution. This could be due to the crosslinked structure of the adsorbent. After five cycles, the recoveries of La(III), Ce(III), and Eu(III) were measured as 46.40, 45.70, and 47.20 mg/L, respectively. Collectively, these results demonstrate that the CS-EDTA-GL adsorbent is stable and reusable for the recovery of REEs from aqueous solutions.

3.8 Interfering ions effect

The effect of interfering ions, including Na^+, K^+, Ca^{2+}, and Mg^{2+}, was investigated due to their frequent occurrence in both natural water and industrial wastewater contaminated with REEs. The concentration ratios of K^+, Na^+, Ca^{2+}, and Mg^{2+} to La(III) ions ($C/CLa_{(III)}$) were 0, 5, 10, 20, 50, and 100, respectively. These ions may compete for the active adsorption sites on the CS-EDTA-GL adsorbent, potentially reducing the REE removal efficiency. Figure 6(b) illustrates the influence of these cations on the removal efficiency of La(III), demonstrating that no significant reduction in the removal efficiency was observed at lower interfering ion concentrations. However, a slight decrease in the adsorption efficiency was noted as concentrations increased from 0 to 100 C/La(III), with values dropping from 98.80% to 85.20%, 98.10% to 85.50%, 98.10% to 84.1%, and 96.10% to 84.90% for the La(III) ion in the presence of Na^+, K^+, Ca^{2+}, and Mg^{2+} interfering ions, respectively. These findings suggest that the adsorption performance of CS-EDTA-GL was only marginally affected by the presence of interfering ions.

3.9 Adsorption mechanism

For REE adsorption, various mechanisms, including electrostatic attraction and complexation, have been reported using different functional groups, such as the hydroxyl, amine, and carboxyl groups (Feng et al., 2021). The pH_{PZC} of CS-EDTA-GL was 3.6 owing to the introduction of EDTA groups into CS and GL during the crosslinking process. Based on the isoelectric point and pH effect, the adsorbent surface was positive below isoelectric point, and the $–NH_2$, –OH, and EDTA functional groups were protonated, which led to electrostatic repulsion with the trivalent REEs. Meanwhile, at pH values above this isoelectric point, the surface becomes negative, and all functional groups become deprotonated, which leads to electrostatic interactions toward the REEs. According to previously reported thermodynamic data (Pettit and Powell, 2006), EDTA exists in various species, as denoted by H_nEDTA^{n-4}, where n ranges from 1 to 5. Therefore,

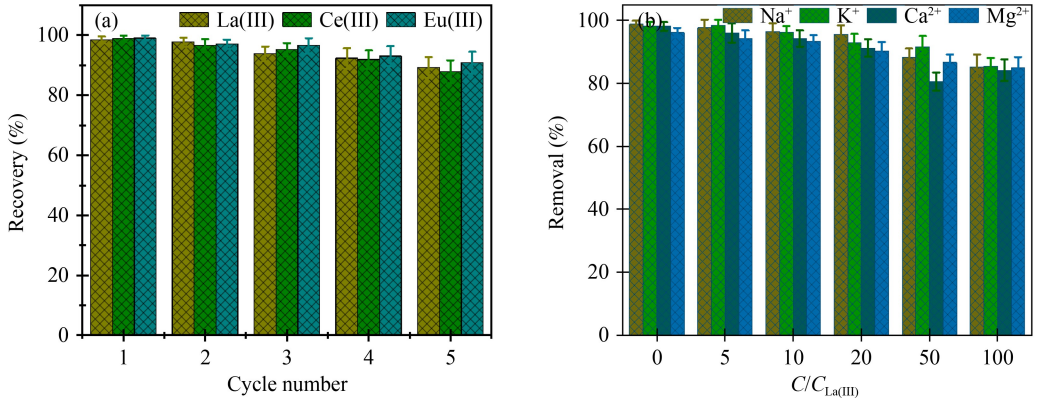

Fig. 6 Regeneration and reusability performance of CS-EDTA-GL in REEs adsorption–desorption cycles (a) and the effect of interfering ions, such as Na^+, K^+, Mg^{2+}, and Ca^{2+}, on the adsorption of La(III) ions onto the CS-EDTA-GL adsorbent (b).

REEs can be adsorbed onto CS-EDTA-GL by these species (Nash et al., 2012).

Equation (1) illustrates the significant roles of chelation and complexation in the adsorption of REEs. A similar type of adsorption behavior was reported by Zhao et al. (2016) for REE adsorption onto the EDTA-β-CD adsorbent:

$$RR'H_iEDTA^{i-3} + Ln(III) \rightleftharpoons (RR'EDTA)Ln + iH^+ \quad (1)$$

where R and R` are CS and GL, respectively, and i is the H-numbers in EDTA, which ranges from 2 to 3.

Several characterization techniques, including EDS, elemental mapping, XPS, and FT-IR, were employed to investigate the REE removal mechanism by comparing the adsorbent before and after the adsorption. Figure S6 shows the elemental mapping and compositional results of CS-EDTA-GL after the simultaneous adsorption of La(III), Ce(III), and Eu(III). The mappings display uniform and colorful spots throughout the images, confirming the presence of well-distributed REE adsorption sites. Additionally, the elemental distribution and composition revealed a higher adsorption of Eu(III) than that of La(III) and Ce(III), which is consistent with the results of the isotherm analysis. These results corroborate the findings of the multi-component adsorption section. To further verify

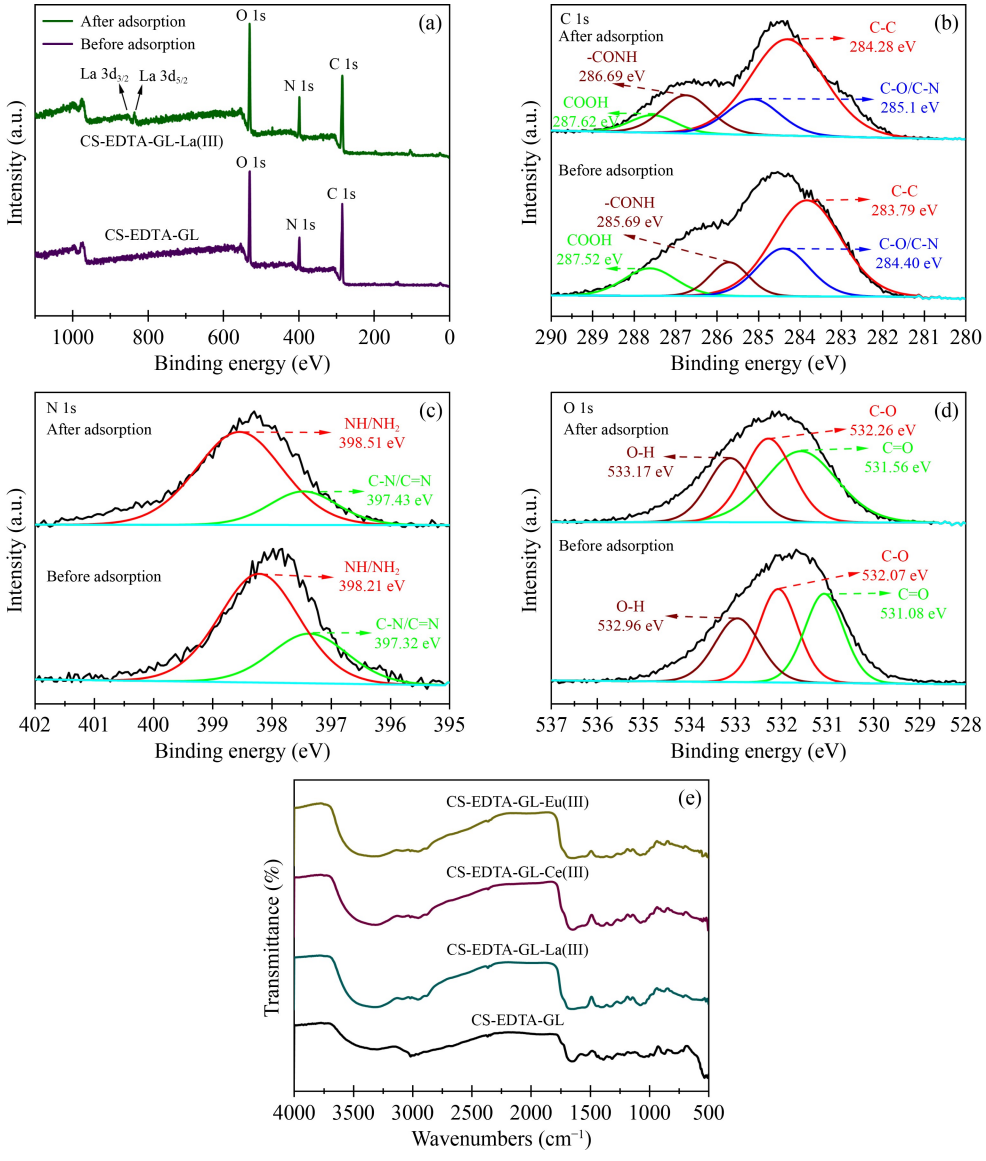

Fig. 7 Full-scanned XPS spectra (a); high resolution XPS spectra of C 1s (b), N 1s (c), and O 1s (d); and FTIR spectra (e) of the CS-EDTA-GL surface before and after La(III) adsorption.

the REE adsorption mechanism for the CS-EDTA-GL adsorbent, the XPS full-scan survey spectra of La(III) ion adsorption were recorded, as shown in Fig. 7(a). Before adsorption, CS-EDTA-GL exhibited binding energy peaks at 284.20, 397.22, and 529.78 eV, corresponding to C 1s, N 1s, and O 1s, respectively. After the adsorption of La(III) ions, two new energy bands appeared at approximately 835.5 and 854.8 eV, corresponding to the energy bands of La $3d_{5/2}$ and La $3d_{3/2}$, respectively. These additional peaks demonstrate the successful adsorption of La(III) ions onto CS-EDTA-GL adsorbent (Wu et al., 2022). High-resolution spectra of C 1s, N 1s, and O 1s were recorded before and after the adsorption of La(III) ions to gain a comprehensive understanding of the adsorption mechanism, as shown in Figs. 7(b)–7(d), respectively. Before adsorption, the high-resolution C 1s spectrum (Fig. 7(b)) displayed four peaks at approximately 283.79, 284.40, 285.69, and 287.58 eV, corresponding to C−C, C−O/C−N, −CONH, and −COOH, respectively. After La(III) adsorption, these peaks shifted slightly toward high energies with reduced intensities at 284.28, 285.1, 286.69, and 287.62 eV, respectively, confirming the involvement of C=O of the −COOH and −CONH groups in La(III) adsorption via coordination complexation (Shen et al., 2021). The N 1s high-resolution spectrum (Fig. 7(c)) exhibited two peaks at 397.32 and 398.21 eV, corresponding to the C−N/C=N and NH/NH_2 groups, respectively. After La(III) adsorption, these peaks were slightly shifted toward high binding energies with a significant decrease in peak intensity at 397.43 and 398.51 eV, respectively, attributed to electrostatic interactions between the N atom and La(III) ions (Ma et al., 2021). In the high-resolution O 1 s spectrum (Fig. 7(d)), the peaks at 531.08, 532.07, and 532.96 eV were attributed to C=O, C−O, and O−H binding, respectively. After La(III) adsorption, these peaks slightly shifted toward high binding energy at 531.56, 532.26, and 533.17 eV with reduced intensities, confirming the formation of strong chelation between O atoms and La(III) ions (Yan et al., 2023). Additionally, electron sharing between the O and N atoms with the La(III) atoms reduced the electron density cloud of the O and N atoms, which resulted in an increase in the binding energy, as shown in the high-resolution O and N atom spectra, consistent with previous reports (He et al., 2015). In support of the XPS results, the FT-IR spectra before and after REE adsorption are shown in Fig. 7(e), indicating a shift of 1643 cm^{-1} (C=O) toward ~1515 cm^{-1}. Moreover, the overlapping peaks of −OH and $-NH_2$ at 3300 cm^{-1} became weaker, confirming the interaction between the −COOH and $-NH_2$ groups and the REE ions via coordination complexation. A similar behavior was previously reported by our research group in the adsorptive removal of heavy metal ions onto a GO-EDTA-CS adsorbent through electrostatic interactions and coordination complexation (Verma et al., 2022c, 2022d).

3.10 Adsorption performance of CS-EDTA-GL in pure water, tap water, and industrial wastewater

From a practical perspective, the performance of the prepared adsorbent was carried out in DI water, tap water, and industrial wastewater samples; the wastewater was collected from two locations in Republic of Korea (details provided in Text SI−3.5). Due to the challenges in analyzing REEs at environmental-level concentrations and the absence of certified reference values for industrial wastewater, the samples were intentionally spiked with REEs at 100 μg/L. Table S1 presents the calculated REE concentrations in the treated wastewater, which demonstrates the effective removal of REEs. Furthermore, the recovery of all REEs from the wastewater was sufficiently high (< 96%), validating the practical applicability of the CS-EDTA-GL adsorbent for the treatment of REE-contaminated wastewater. These results confirm the high reliability of the CS-EDTA-GL adsorbent for the treatment of wastewater containing REEs.

A comparison of the maximum adsorption capacities of the synthesized CS-EDTA-GL adsorbent with those of commonly used adsorbents is summarized in Table 4. The CS-EDTA-GL adsorbent exhibited a better adsorption capacity than most previously reported adsorbents, suggesting its relative efficiency for removing REEs from water. Brown marine algae exhibit an exceptionally high adsorption capacity for REEs, which is likely due to the availability of a large number of carboxylic groups on their surfaces (Vijayaraghavan et al., 2010).

4 Conclusions

In summary, the synthesized CS-EDTA-GL adsorbent demonstrated significant potential for the removal of trivalent REEs from water via adsorption. The Langmuir isotherm model fitting confirmed monolayer adsorption, with adsorption capacities of 76.70 ± 5.70, 79.10 ± 6.80, and 86.20 ± 5.10 mg/g for La(III), Ce(III), and Eu(III), respectively. The adsorption process reached equilibrium within 90 min, and the kinetic data fit well with the PSO kinetic model, confirming the chemisorption process. In a ternary

Table 4 Comparison of maximum adsorption capacities of CS-EDTA-GL adsorbents with other adsorbents for REE removal

Adsorbent	REEs	q_m (mg/g)	Isotherm fitting	Ref.
BC@FeNPs-EPS	Eu(III)	23.39	Langmuir	Yan et al., 2023
2D Zn-BDC MOF/GO	La(III)	36.82	Langmuir	Chen et al., 2022
GO/P(NIPAM-MA)	La(III)	33.1	Langmuir	Yang et al., 2020
CMPO@MIL-101(Cr)	Eu(III)	12.5	Langmuir	Perumal et al., 2019
GO-$TAPA_{1:2}$	La(III)	11.24	Langmuir	Huang et al., 2014
Fe_3O_4(humic acid)	Eu(III)	10.6	Langmuir	González et al., 2018
Saccharomyces cerevisiae-immobilized cross-linked cellulose	Eu(III)	25.91	Langmuir	Arunraj et al., 2019
TpPa COFs	La(III)	84.67	Langmuir	Xiao et al., 2022
Platanus orientalis leaf powder	La(III) Ce(III)	28.65 32.05	Langmuir Langmuir	Sert et al., 2008
Brown marine alga	La(III Ce(III) Eu(III)	150.04[a)] 147.11[a)] 132.20[a)]	Langmuir Langmuir Langmuir	Li et al., 2004
EDTA-*β*-CD	La(III Ce(III) Eu(III)	47.64 49.45 55.46	Langmuir Langmuir Langmuir	Zhao et al., 2016
CS-EDTA-GL	La(III Ce(III) Eu(III)	76.70 ± 5.70 79.10 ± 6.80 86.20 ± 5.10	Langmuir Langmuir Langmuir	This work

Notes: a) converted unit.

mixed solution of REEs, Eu(III) exhibited faster adsorption than Ce(III) and La(III), despite no significant differences in the adsorption behavior in single-component systems. The adsorption mechanism showed both electrostatic and coordination complexation roles in REE adsorption. Finally, CS-EDTA-GL could successfully adsorb REEs in real wastewater treatment, with excellent recovery over six continuous adsorption–desorption cycles, demonstrating its strong potential as a promising material for practical applications in the removal of REEs from wastewater.

CRediT Authorship Contribution Statement

M. Verma: Conceptualization, experiments, writing original draft; **D. Sachan:** experiments; **V. Kumar, W. Ahmad, N. Sharma:** Editing, **H. Kim:** investigation and review.

Conflict of Interests The authors declare that the research was conducted in the absence of any commercial or financial relationships that could be construed as a potential conflict of interest.

Acknowledgements Monu Verma would like to thank the National Research Foundation of Korea (NRF) for funding provided by the Ministry of Science and ICT through the Brain Pool Program (RS-2024-00406513). This study was supported by the Green Venture R&D program (S3051540) funded by the Ministry of SMEs and Startups (MSS, Republic of Korea). This study was supported by the Strategic Academic Leadership Program of RUDN University, Russia.

Electronic Supplementary Material Supplementary material is available in the online version of this article at https://doi.org/10.1007/s11783-025-1971-1 and is accessible for authorized users.

References

Aoki N, Nishikawa M, Hattori K (2003). Synthesis of chitosan derivatives bearing cyclodextrin and adsorption of p-nonylphenol and bisphenol A. Carbohydrate Polymers, 52(3): 219–223

Arunraj B, Sathvika T, Rajesh V, Rajesh N (2019). Cellulose and saccharomyces cerevisiae embark to recover europium from phosphor powder. ACS Omega, 4(1): 940–952

Brewer A, Chang E, Park D M, Kou T, Li Y, Lammers L N, Jiao Y (2019). Recovery of rare earth elements from geothermal fluids through bacterial cell surface adsorption. Environmental Science & Technology, 53(13): 7714–7723

Brown A T, Balkus K J Jr (2021). Critical rare earth element recovery from coal ash using microsphere flower carbon. ACS Applied Materials & Interfaces, 13(41): 48492–48499

Chen B, Zhao H, Chen S, Long F, Huang B, Yang B, Pan X (2019). A magnetically recyclable chitosan composite adsorbent functionalized with EDTA for simultaneous capture of anionic dye and heavy metals in complex wastewater. Chemical Engineering Journal, 356: 69–80

Chen Z, Li Z, Chen J, Tan H, Wu J, Qiu H (2022). Selective adsorption of rare earth elements by Zn-BDC MOF/graphene oxide nanocomposites synthesized via *in situ* interlayer-confined strategy. Industrial & Engineering Chemistry Research, 61(4): 1841–1849

Dupont D, Brullot W, Bloemen M, Verbiest T, Binnemans K (2014). Selective uptake of rare earths from aqueous solutions by EDTA-functionalized magnetic and nonmagnetic nanoparticles. ACS Applied Materials & Interfaces, 6(7): 4980–4988

Feng S, Du X, Bat-Amgalan M, Zhang H, Miyamoto N, Kano N (2021). Adsorption of REE from aqueous solution by EDTA-chitosan modified with zeolite imidazole framework (ZIF-8). International Journal of Molecular Sciences, 22(7): 3447

Gismondi P, Kuzmin A, Unsworth C, Rangan S, Khalid S, Saha D (2022). Understanding the adsorption of rare-earth elements in oligo-grafted mesoporous carbon. Langmuir, 38(1): 203–210

González J A, Bafico J G, Villanueva M E, Giorgieri S A, Copello G J (2018). Continuous flow adsorption of ciprofloxacin by using a nanostructured chitin/graphene oxide hybrid material. Carbohydrate Polymers, 188: 213–220

Hamza M F, Guibal E, Abdel-Rahman A A, Salem M, Khalafalla M S, Wei Y, Yin X (2022). Enhancement of cerium sorption onto urea-functionalized magnetite chitosan microparticles by sorbent sulfonation: application to ore leachate. Molecules, 27(21): 7562

He R, Li W, Deng D, Chen W, Li H, Wei C, Tang Y (2015). Efficient removal of lead from highly acidic wastewater by periodic ion imprinted mesoporous SBA-15 organosilica combining metal coordination and co-condensation. Journal of Materials Chemistry. A, 3(18): 9789–9798

Huang L, Wang M, Shi C, Huang J, Zhang B (2014). Adsorption of tetracycline and ciprofloxacin on activated carbon prepared from lignin with H_3PO_4 activation. Desalination & Water Treatment, 52(13−15): 2678–2687

Ji B, Zhang W (2022). Adsorption of cerium (III) by zeolites synthesized from kaolinite after rare earth elements (REEs) recovery. Chemosphere, 303(1): 134941

Johlin J M (1930). The isoelectric point of gelatin and its relation to the minimum physical properties of gelatin. Journal of Biological Chemistry, 86(1): 231–243

Jun B M, Kim H H, Rho H, Seo J, Jeon J W, Nam S N, Min P C, Yoon Y (2023). Recovery of rare-earth and radioactive elements from contaminated water through precipitation: a review. Chemical Engineering Journal, 475: 146222

Kegl T, Košak A, Lobnik A, Novak Z, Kralj A K, Ban I (2020). Adsorption of rare earth metals from wastewater by nanomaterials: a review. Journal of Hazardous Materials, 386: 121632

Li H, Meng B, Chai S H, Liu H, Dai S (2016). Hyper-crosslinked *β*-cyclodextrin porous polymer: an adsorption-facilitated molecular catalyst support for transformation of water-soluble aromatic molecules. Chemical Science, 7(2): 905–909

Li S, Hu B, Jiang Z, Liang P, Li X, Xia L (2004). Selective separation of La^{3+} and lanthanum organic complexes with nanometer-sized titanium dioxide and their detection by using fluorination-assisted electrothermal vaporization ICP-AES with *in-situ* matrix removal. Environmental Science & Technology, 38(7): 2248–2251

Li X Z, Zhou L P, Yan L L, Dong Y M, Bai Z L, Sun X Q, Diwu J, Wang S, Bünzli J C, Sun Q F (2018). A supramolecular lanthanide separation approach based on multivalent cooperative enhancement of metal ion selectivity. Nature Communications, 9(1): 547

Lone S, Yoon D H, Lee H, Cheong I W (2019). Gelatin-chitosan hydrogel particles for efficient removal of Hg(II) from wastewater. Environmental Science: Water Research & Technology, 5(1): 83–90

Ma Z, Li F, Jia A, Zhang X, Wang Y (2021). Facile synthesis of EDTA grafted 3D spherical-chain porous silica with high capacity for rapidly selective adsorption of Cu(II) from aqueous solutions. Journal of Porous Materials, 28(1): 299–310

Maes S, Zhuang W Q, Rabaey K, Alvarez-Cohen L, Hennebel T (2017). Concomitant leaching and electrochemical extraction of rare earth elements from monazite. Environmental Science & Technology, 51(3): 1654–1661

Nash K L, Brigham D, Shehee T C, Martin A (2012). The kinetics of lanthanide complexation by EDTA and DTPA in lactate media. Dalton Transactions, 41(48): 14547–14556

Park J H, Kim H, Kim M, Lim J M, Ryu J, Kim S (2020). Sequential removal of radioactive Cs by electrochemical adsorption and desorption reaction using core-shell structured carbon nanofiber–Prussian Blue composites. Chemical Engineering Journal, 399: 125817

Pathapati S V S H, Free M L, Sarswat P K (2023). A comparative study on recent developments for individual rare earth elements separation. Processes, 11(7): 2070

Pearson R G (1963). Hard and soft acids and bases. Journal of the American Chemical Society, 85(22): 3533–3539

Perumal S, Atchudan R, Yoon D H, Joo J, Cheong I W (2019). Spherical chitosan/gelatin hydrogel particles for removal of multiple heavy metal ions from wastewater. Industrial & Engineering Chemistry Research, 58(23): 9900–9907

Pettit L D, Powell K (2006). IUPAC Stability Constants Database. New York UK: IUPAC

Rahman R O A, Ibrahium H A, Hung Y T (2011). Liquid radioactive wastes treatment: a review. Water, 3(2): 551–565

Ren S, Yang X, Tang L, Du X, Li M, Yin X (2023). A chitosan-based Y^{3+}-imprinted hydrogel with reversible thermo-responsibility for the recovery of rare earth metal. Applied Surface Science, 611: 155602

Repo E, Warchol J K, Kurniawan T A, Sillanpää M E T (2010). Adsorption of Co(II) and Ni(II) by EDTA- and/or DTPA-modified chitosan: kinetic and equilibrium modeling. Chemical Engineering Journal, 161(1−2): 73–82

Roosen J, Binnemans K (2014). Adsorption and chromatographic separation of rare earths with EDTA- and DTPA-functionalized chitosan biopolymers. Journal of Materials Chemistry. A, 2(5): 1530–1540

Sert Ş, Kütahyali C, İnan S, Talip Z, Çetinkaya B, Eral M (2008). Biosorption of lanthanum and cerium from aqueous solutions by *Platanus orientalis* leaf powder. Hydrometallurgy, 90(1): 13–18

Shen J, Liang C, Zhong J, Xiao M, Zhou J, Liu J, Liu J, Ren S (2021). Adsorption behavior and mechanism of *Serratia marcescens* for Eu(III) in rare earth wastewater. Environmental Science & Pollution Research International, 28(40): 56915–56926

Sirviö J A, Kantola A M, Komulainen S, Filonenko S (2021). Aqueous modification of chitosan with itaconic acid to produce strong oxygen barrier film. Biomacromolecules, 22(5): 2119–2128

Tülü M, Geckeler K E (1999). Synthesis and properties of hydrophilic polymers. Part 7. Preparation, characterization and metal complexation of carboxy-functional polyesters based on poly(ethylene glycol). Polymer International, 48(9): 909–914

Unsworth C E, Kuo C C, Kuzmin A, Khalid S, Saha D (2020). Adsorption of rare earth elements onto DNA-functionalized mesoporous carbon. ACS Applied Materials & Interfaces, 12(38): 43180–43190

Verma M, Ahmad W, Park J H, Kumar V, Vlaskin M S, Vaya D, Kim H (2022a). One-step functionalization of chitosan using EDTA: kinetics and isotherms modeling for multiple heavy metals adsorption and their mechanism. Journal of Water Process Engineering, 49: 102989

Verma M, Borah R, Kumar A, Chae S H, Pan S Y, Kumar V, Vlaskin M S, Kim H (2022b). Capturing of inorganic and organic pollutants simultaneously from complex wastewater using recyclable magnetically chitosan functionalized with EDTA adsorbent. Process Safety & Environmental Protection, 167: 56–66

Verma M, Kumar A, Lee I, Kumar V, Park J H, Kim H (2022c). Simultaneous capturing of mixed contaminants from wastewater using novel one-pot chitosan functionalized with EDTA and graphene oxide adsorbent. Environmental Pollution, 304: 119130

Verma M, Lee I, Hong Y, Kumar V, Kim H (2022d). Multifunctional *β*-cyclodextrin-EDTA-chitosan polymer adsorbent synthesis for simultaneous removal of heavy metals and organic dyes from wastewater. Environmental Pollution, 292(B): 118447

Verma M, Lee I, Kumar V, Pan S Y, Fan C, Kim H (2023). Chitosan cross-linked *β*-cyclodextrin polymeric adsorbent for the removal of perfluorobutanesulfonate from aqueous solution: adsorption kinetics, isotherm, and mechanism. Environmental Science & Pollution Research International, 30(7): 19259–19268

Vijayaraghavan K, Sathishkumar M, Balasubramanian R (2010). biosorption of lanthanum, cerium, europium, and ytterbium by a brown marine alga, *Turbinaria conoides*. Industrial & Engineering Chemistry Research, 49(9): 4405–4411

Vijayaraghavan K, Sathishkumar M, Balasubramanian R (2011). Interaction of rare earth elements with a brown marine alga in multi-component solutions. Desalination, 265(1−3): 54–59

Wu L, Yang M, Yao L, He Z, Yu J X, Yin W, Chi R A (2022). Polyaminophosphoric acid-modified ion-imprinted chitosan aerogel with enhanced antimicrobial activity for selective La(III)) recovery and oil/water separation. ACS Applied Materials & Interfaces, 14(48): 53947–53959

Xiao J, Li B, Qiang R, Qiu H, Chen J (2022). Highly selective adsorption of rare earth elements by honeycomb-shaped covalent organic frameworks synthesized in deep eutectic solvents. Environmental Research, 214(4): 113977

Xie X, Tan X, Yu Y, Li Y, Wang P, Liang Y, Yan Y (2022). Effectively auto-regulated adsorption and recovery of rare earth elements via an engineered *E. coli*. Journal of Hazardous Materials, 424(C): 127642

Yan Q, Yang Y, Chen W, Weng X, Owens G, Chen Z (2023). Recovery and removal of rare earth elements from mine wastewater using synthesized bio-nanoparticles derived from *Bacillus cereus*. Chemical Engineering Journal, 459: 141585

Yang X, Debeli D K, Shan G, Pan P (2020). Selective adsorption and high recovery of La^{3+} using graphene oxide/poly (N-isopropyl acrylamide-maleic acid) cryogel. Chemical Engineering Journal, 379: 122335

Zhang H, Li R, Zhang Z (2022). A versatile EDTA and chitosan bi-functionalized magnetic bamboo biochar for simultaneous removal of methyl orange and heavy metals from complex wastewater. Environmental Pollution, 293: 118517

Zhao F, Repo E, Meng Y, Wang X, Yin D, Sillanpää M (2016). An EDTA-*β*-cyclodextrin material for the adsorption of rare earth elements and its application in preconcentration of rare earth elements in seawater. Journal of Colloid & Interface Science, 465: 215–224

Zhao F, Repo E, Yin D, Chen L, Kalliola S, Tang J, Iakovleva E, Tam K C, Sillanpää M (2017). One-pot synthesis of trifunctional chitosan-EDTA-*β*-cyclodextrin polymer for simultaneous removal of metals and organic micropollutants. Scientific Reports, 7(1): 15811